Spectral and mineralogical alteration process of naturally-heated carbonaceous chondrites

M. Matsuoka[1], T. Nakamura[2], N. Miyajima[3], T. Hiroi[4], N. Imae[5], A. Yamaguchi[5]

[1]ISAS/JAXA, Sagamihara, Kanagawa 252-5210, Japan (matsuoka.moe@jaxa.jp),

[2]Tohoku University, Sendai, Miyagi 980-8578, Japan,

[3]Bayerisches Geoinstitut, University of Bayreuth, Bayreuth 95440, Germany,

[4]Brown University, Providence, RI 02912, USA,

[5]Research National Institute of Polar Research, Tachikawa, Tokyo 190-8518, Japan.

Abstract

Spectral and mineralogical analyses were performed using nine naturally hydrated and dehydrated carbonaceous chondrite samples which were classified into heating stages (HS) from I to IV based on previous X-ray diffraction results. In-situ heating of samples at 120–400 °C was performed during spectral measurements and successfully removed absorbed water and part of rehydrated water from chondrite samples. Reflectance spectra of HS-I samples show the positive slope in visible (Vis)-infrared (IR) range and the significant 0.7- and 3-μm absorption bands. The 0.7-μm band appears in only HS-I sample spectra. With increasing temperature of heating, (1) Vis-IR slope decreases, (2) the 3-μm band becomes shallower, and (3) Christiansen feature (CF) and Reststrahlen bands (RB) shift toward longer wavelength. TEM-EDX analyses showed that the matrix of strongly-heated chondrites consists of tiny olivine, low-Ca pyroxene, and FeNi metallic particles mostly smaller than 100 nm in diameter, instead of Fe-rich serpentines and tochilinite observed in the HS-I chondrite. Therefore, in proportion to the heating degree, amorphization and dehydration of serpentine and tochilinite from HS-I to HS-II may cause the 0.7- and 3-μm band weakening, spectral bluing and darkening of chondrite spectra. In addition, formation of secondary anhydrous silicates and FeNi-rich metal grains at HS-IV would be responsible for the 3-μm band depth decrease, spectral reddening and brightening, CF peak shift, and RB changes of chondrite spectra. Those spectral changes in response to mineralogical alteration processes will be useful to interpret planetary surface composition by remote-sensing observations using ground-based or airborne/space telescopes or spacecraft missions.

1. Introduction

C-type asteroids are thought to be parent bodies of CM chondrites based on spectroscopic studies: C-type asteroids and CM chondrites both show similar reflectance spectra in Ultraviolet (UV) - visible (Vis) - near-infrared (NIR) range (e.g., Burbine et al., 2002; Hiroi et al., 1993, 1996; Lantz et al., 2013; Takir et al., 2013; Vilas, 1994; Vilas & Gaffey, 1989). It is known that many carbonaceous chondrites and C-type asteroids experienced low-temperature hydration which results in the formation of hydrated phases.

On the other hand, several C-type asteroids are thought to have been dehydrated by hearting or impact events after such aqueous alteration judging from their spectra which are slightly different from the spectra of fresh or space-weathered chondrites but similar to the spectra of experimentally-heated chondrites (Hiroi et al., 1993, 1996). The asteroid explorer Hayabusa2 of the Japan Aerospace Exploration Agency (JAXA), launched on December 3, 2014, and have performed remote sensing observations at the target C-type asteroid 162173 Ryugu for 1.5 years. Vis-NIR spectra of Ryugu global surface are similar to those of moderately-heated or shocked carbonaceous chondrites (Kitazato et al., 2019a; Sugita et al., 2019); little 0.7-μm absorption band, which arises from Fe^{3+}-Fe^{2+} charge transfers in Fe-rich hydrous silicates except for pole regions (Tatsumi et al. 2021, submitted), and a weak but sharp 2.72-μm absorption (Kitazato et al., 2019b). It is also suggested that Ryugu surface previously experienced greater solar heating or solar wind implantation before settling in its current orbit (Morota et al., 2020). The mineralogical, spectral, and physical analyses of returned samples from Ryugu arriving in December 2020 are expected to provide a strong constraint on the evolution process of the early solar system, and will be performed in near future.

Akai (1992) and Nakamura (2005) reported that more than twenty Antarctic carbonaceous chondrites that have been heated and dehydrated after aqueous alteration processes on their parent bodies, C-type asteroids. Based on the results of X-ray diffraction analyses, they indicated that serpentine became amorphous and secondary olivine crystals grew with increasing heating stage. Nakamura (2005) reported that moderately heated samples, such as Yamato (Y-)793321 and Asuka (A-)881334, show incomplete serpentine decomposition and dehydration based on the absence of serpentine basal reflections and the presence of prism reflections. The samples classified as a higher

heating stage show diffraction patterns of olivine without prism reflection of serpentine, indicating secondary olivine crystallized at the expense of serpentine. Spectral analyses of experimentally heated Murchison samples showed spectral changes such as the 0.7- and 3-μm absorption band decrease (Hiroi et al., 1993, 1996; Mogi et al., 2017; Yamashita et al., 2015). However, spectral properties of naturally-heated carbonaceous chondrites are still unclear. In this study, spectral analysis in the Vis-NIR range and mineralogical analysis in the micro scale using several naturally-heated carbonaceous chondrites classified into various heating stages (HS) defined by Nakamura (2005) are performed to clarify the relationship between spectral and mineralogical properties affected by heating.

2. Samples and analytical procedures

2.1. Samples

Samples of five CM chondrites, three CY chondrites, and one CV chondrite were used in this study. The meteorite samples are classified into four classes according to the degree of heating defined by Nakamura (2005) based on the results of X-ray diffraction analyses as follows.

1. Heating Stage (HS)-I: Unheated (<300 °C) carbonaceous chondrites. Hydrous phases are mainly composed of serpentine and tochilinite. Murchison CM2 and Murray CM2 are classified into this class.
2. HS-II: Moderately heated (300–500 °C) carbonaceous chondrites. Serpentine is decomposed to poorly crystalline on an amorphous state. Dehydration is incomplete. Y-793321 CM2, Jbilet Winselwan CM2, Y 982086 CM2, and Y 980115 CY are in this class.
3. HS-IV: Strongly heated (>750 °C) carbonaceous chondrites. Hydrous minerals are almost completely dehydrated, and secondary anhydrous minerals that formed at the expense of amorphous silicates are dominant. Belgica (B-) 7904 CY and Y-86720 CY are in this class.
4. Anhydrous: Carbonaceous chondrites that consist of anhydrous minerals almost entirely exclusive of hydrous minerals. Allende CV3 is in this class.

Meteorite chips were powdered with a tungsten carbide mortar and a pestle, and passed through a sieve to make a particle size fraction of 77 μm or smaller for Murray, Y-793321,

and B-7904, and 155 μm or smaller for the other meteorite samples. Each powder sample was placed in an alumite-coated dish of 30 mm in diameter and flattened by tapping on the side of the dish.

In addition, LEW87022 (unheated CM), Jbilet Winselwan, Dhofar 735 (heated at 600–900 °C; the temperature range was estimated by Nakato et al. (2009), and Murchison experimentally heated at 900 °C (Mogi et al., 2017; Yamashita et al., 2015) were used for transmission electron microscope (TEM) analysis.

2.2. Analytical methods

2.2.1. Spectral measurements

The reflectance spectra of meteorite samples were measured over the wavelength range of 0.38–15 μm in vacuum condition at <2 hPa using Bruker VERTEX 70v Fourier Transform Infrared (FT-IR) spectrometer at Tohoku University. The spectral resolution were 32, 16, 8, and 4 cm^{-1} for 0.38–0.56, 0.55–1.10, 1.05–2.20, and 2.10–15 μm in wavelength, respectively. The light sources were a xenon lamp for 0.38–0.56 μm, a halogen lamp for 0.55–2.20 μm, and a globar infrared source for 2.10-15 μm. For Y-86720 and Allende, four wavelength range of each setting is 0.38–0.56, 0.55–1.10, 1.05–2.70, and 2.65–15 μm in wavelength, respectively. The incidence and emergence angles were set to 30 and 0°, respectively. The measured surface area was ~5 mm in diameter. The reflectance standards were Spectralon (SRS99, Labsphere) and Infragold. Infrared spectra of samples were measured by stepwise heating at 120, 160, 200, 240, 280, 320, 360, and 400 °C, in order to remove terrestrial water, i.e., rehydrated water, tightly bound to the silicate structure compared with the adsorbed water (e.g., Mogi et al., 2017), and adsorbed water. Murchison and Murray were heated only to 120 °C for removal of adsorbed water to avoid any thermal alteration of hydrous minerals.

2.2.2. Field emission scanning electron microscope (FE-SEM) and transmission electron microscope (TEM) analysis

The meteorite chip samples (LEW87022, Jbilet Winselwan, Dhofar 735, and Murchison experimentally heated at 900 °C) were cut and embedded as the cross section up in an epoxy resin. They are polished and observed using FE-SEM (JEOL JSM-7001F)

125 at Tohoku University for chemical analysis and sampling site selection for TEM analyses.
126 The ultrathin sections ~100 nm in thickness were prepared from selected areas using a
127 dual beam focused ion milling machine with Ga ion and electron beams (FEI Scios) at
128 Bayerisches Geoinstitut, University of Bayreuth (BGI, Univ Bayreuth), and placed on a
129 TEM Cu grid. The microscopic analysis was performed using a scanning transmission
130 electron microscope (TEM: FEI Titan G2 80-200 S/TEM) equipped with energy
131 dispersive X-ray (EDX) spectrometers (or system) at BGI, Univ Bayreuth.
132
133 # 3. Results
134 ## 3.1. The in-situ heating effects for the 3-μm absorption band
135 Figure 1a–i shows the changes of reflectance spectra of all meteorite samples
136 measured during in-situ heating at 120–400 °C. The 3-μm band of all spectra heated at
137 400 °C shows the shallowest depth, e.g., The 3-μm band depth of HS-II and IV chondrites
138 reduced down to nearly one third compared to that of unheated sample spectrum (e.g.,
139 Fig. 1c, f, g, and h). The position of the 3-μm band appears around at 2.9 μm of spectra
140 measured unheated condition, and in proportion to heating temperature, shifts toward
141 shorter wavelength, then appears at nearly 2.8 μm as shown in spectra measured at 400 °C
142 heating. It indicates that adsorbed water of meteorite samples was removed by in-situ
143 heating spectra measurements. Organic absorption bands due to C-H stretching mode
144 appear obviously around 3.4–3.5 μm especially heated sample spectra.
145
146 ## 3.2. Reflectance spectra of hydrated and dehydrated carbonaceous chondrites
147 Figure 2a and b shows all the reflectance spectra of meteorite samples, and in
148 infrared range, we take spectra measured by in-situ heating at 120 °C. Reflectance spectra
149 of HS-I samples have positive Vis-IR slope as one shoulder of UV absorption centered at
150 <0.25 μm possibly due to π-π* plasmon resonance in polycyclic aromatic hydrocarbon
151 (PAH) components (Duley & Lazarev, 2004; Lyuba Moroz et al., 2004) and/or Fe-O and
152 Ti-O charge transfers (Cloutis et al., 2008). HS-I spectra also show the absorption band
153 around 0.7 μm (Fig. 2b), which arises from Fe^{3+}-Fe^{2+} charge transfers in phyllosilicates.
154 The Vis reflectance decreases from HS-I to HS-II, and then increases to HS-IV and
155 anhydrous Allende: e.g., reflectance at 0.55 μm in wavelength of HS-I samples is higher

than ~4.5%, that of HS-II samples decreases to ~3%, and then that of HS-IV samples increases to over 4% (Fig. 2b and Table 1). On the other hand, the spectral slope in Vis-IR range decreases continuously with increasing heating-degree from HS-I to HS-IV (Fig. 2b and Table 1).

The 3-μm band due to O-H stretching vibration (Ryskin, 1974) in hydrous minerals is apparently shown in HS-I samples, and becomes shallower with increasing heating degree (Figs. 1a–i and 3a–c). For band depth calculation, continuum removal is performed by dividing each spectrum measured at 120 and 400 °C by a linear continuum tangent to the spectrum on both edges of the 3-μm band, at ~2.5 and 4.0 μm. The band depth and peak wavelength are summarized in Table 1. The band center shifts from ~2.81 μm of HS-I (120 °C heating) and to ~2.77 μm of HS-II (400 °C heating), and finally toward ~2.88 μm of HS-IV and Allende (400 °C heating) as shown in Fig. 3b, 3c, and Table 1. Regarding Jbilet Winselwan, it exhibits a unique sharp absorption band with a single peak at 2.72 μm. Y 980115 also has a sharp peak at nearly 2.75 μm, which locates at shorter wavelength range compared to the other HS-II samples (Fig. 3b). The 3-μm absorption band depths with increasing heating stage; e.g., ~81% and ~97% shallower at HS-II Y-793321 and HS-IV B-7904, than at HS-I Murray (Fig. 3b, c, and Table 1). We are aware that there is contamination of rehydrated water in each spectrum because even the spectrum of anhydrous sample Allende, which has rare hydrous silicates (Berlanga et al., 2016; Bland et al., 2004; Cloutis et al., 2012; Ma & Rossman, 2009), shows the 3-μm absorption band (Fig. 3c and Table 1). In this study, it is difficult to determine the position of rehydration water in the crystal structure of hydrous silicates.

The triplet band with peaks at 3.37, 3.42, and 3.48 μm due to C-H stretching mode in organics are significantly shown in HS-I and Jbilet Winselwan (e.g., Fig. 3b), and also detected from HS-II and IV, even in anhydrous Allende heated at 400 °C (Fig. 3a–c). It seems that there would be contamination of organic matter. Mogi et al. (2017) reported that experimentally-heated Murchison at >400 °C contained up to 2.49±0.04 wt% carbon, and showed no triplet band of C-H stretching mode. Allende contained less carbon (0.36 wt% in matrix reported by Jarosewich, 1990) compared with heated Murchison but show C-H peaks in Hiroi et al. (1996) and this study. Thus, the C-H peaks shown in Allende spectra in this study possibly contributed by contamination.

In this study, we performed in-situ heating as pointed out in section 3.1 to remove adsorbed water of dehydrated carbonaceous chondrite samples, however, rehydrated water which possibly has relatively strong bonds with tetrahedral-octahedral (T-O) layer of serpentine would be remained partly. See also section 4.2.

The 6-μm absorption band depths are significant in all spectra and composed of a peak at ~6.1 μm due to C=C, C=O, and/or C=N stretching modes, and a peak at ~6.1–6.2 μm (1615–1650 cm^{-1}) due to H-O-H bending vibration (Fig. 4). The peak intensity in shorter wavelength side around ~6.05 μm becomes decreasing with increasing temperature of in-situ heating up to 400 °C. It is indicated that in-situ heating would successfully remove adsorbed molecular water from naturally-heated chondrites.

The Christiansen feature (CF) shifts toward the longer wavelength from ~8.7 to ~9.2 μm with increasing heating stage (Fig. 5). In terms of the Reststrahlen band (RB) due to Si-O stretching mode, HS-I spectra show two peaks appeared around 11.4 and 12.2 μm which is consistent with those of Murchison spectra (e.g., Matsuoka, Nakamura, Hiroi, Okumura, & Sasaki, 2020). In HS-II spectra, an additional peak around 10.7 μm is observed. At HS-II, the peak at 11.4 μm becomes weaker and shifts slightly toward longer wavelength, and finally shown around 11.7 μm at HS-IV. The other peak at 12.2 μm becomes prominent and shifts toward ~12.5 μm in HS-IV spectra.

3.3. Mineralogy of hydrated and dehydrated carbonaceous chondrites

There is a compositional difference between the matrix containing "tochilinite cronstedtite intergrowth (TCI)" (Pignatelli et al., 2016) of unheated chondrites, and the matrix of heated chondrites. Heating process facilitates amorphization and dehydration of phyllosilicates and tochilinite in hydrous chondrites. For detailed investigation of chemical and mineralogical changes due to heating process, LEW87022 (HS-I), Jbilet Winselwan (HS-II), Dhofar 735 (HS-IV), and Murchison heated at 900 °C (experimentally heated to HS-IV temperature; Mogi et al., 2017; Mogi et al., 2021 submitted) were observed in TEM and analyzed by EDX (Figs. 6 and 7). The matrix of LEW87022 is dominated by Fe-rich serpentine and tochilinite (Figs. 6d, g, h, and 7). In contrast, matrix of Murchison heated at 900 °C and Dhofar 735 consists of anhydrous silicates such as olivine and low-Ca pyroxene, and Fe- and Ni-rich metallic particles

mostly smaller than 100 nm in diameter (Figs. 6b, c, e, f, and 7). In the matrix of LEW87022, S and Ni exist together with Fe as shown in Fig. 8.

The matrices of strongly heated chondrite of Dhofar 735 and Murchison heated at 900 °C show similar average chemical composition to that of LEW87022; a significant difference is that the strongly heated samples consist of Mg-rich anhydrous silicates such as olivine and pyroxene, and FeNi-rich metal grains (Fig. 7). Comparison in the chemical composition of matrix minerals between HS-I and HS-IV samples suggests that metallic FeNi particles formed from Fe provided by Fe-rich hydrous silicates such as cronstedtite and tochilinite, and Ni from Ni-bearing tochilinite, and then the remnants become Fe-poor anhydrous silicates such as Mg-rich olivine and pyroxene during heating process. The Ni contents of metal grains probably depend on the availability of nearby tochilinite as a source mineral.

4. Discussion

4.1. In-situ heating effect on the 3-μm absorption band

Sample heating at 120 to 400 °C during spectral measurements were performed in order to remove terrestrial water from chondrite samples and the results show that heating significantly decreases the 3-μm band depths. Comparison among the 3-μm band shape of spectra measured at room temperature, 120 °C, and 400 °C is performed using the 3-μm band center wavelength and depth of naturally-heated chondrite spectra. The 3-μm band center is defined as follows:

$$3\text{-}\mu\text{m band depth} = 1 - R_{min}$$

where R_{min} stands for the smallest reflectance value in the range of 2.5–4.0 μm of the continuum-removed spectra (Fig. 3a, b, and c).

At 400 °C heating, HS-II and IV spectra show the shallower absorption than that of measured at room temperature and 120 °C heating (Fig. 3a, b, c, and Table 1). This 3-μm band change is consistent with depth decreasing at nearly 6.2 μm due to H-O-H absorption. In-situ heating is effective to reduce terrestrial water features as a part of the 3-μm absorption band components. For each sample spectrum, the 3-μm band becomes sharper and a little shallower as heating temperature becomes higher (Fig. 3a, b, c, and Table 1), which is consistent with the previous results measured by in-situ heating

249 measurements at 300 °C by Beck et al. (2010) and at up to ~200 °C (475 K) by Takir et
250 al. (2013). For the following discussion, we use the spectral data measured by in-situ
251 heating at 120 °C for HS-I to IV, and 400 °C for HS-II to IV. We are aware that the
252 rehydrated water can be strongly combined within the silicate layer structure, and difficult
253 to remove completely by in-situ heating up to 400 °C in this study (e.g., HS-IV sample
254 spectrum; See also Section 4.2).
255
256 **4.2. Mineralogical changes of carbonaceous chondrites due to heating process**
257 In this study, the mineralogical and chemical changes of carbonaceous
258 chondrites due to heating effects on their parent bodies are summarized as follows:
259 (i) [HS-I to II] Hydrous minerals such as Fe-rich serpentines (cronstedtite decomposes at
260 470 °C; Caillère & Hènin, 1957) and tochilinite (decomposes at ~245 °C; Ivanova et al.,
261 2005; Tonui et al., 2002) became amorphous and decomposed.
262 (ii) [at HS-IV] Submicron-size secondary anhydrous silicates were formed as heating
263 processes. The anhydrous silicates are ranging in composition from Mg-rich olivine to
264 pyroxene (Fig. 7c).
265 (iii) [at HS-IV] Metal grains were generally enriched in Fe (Fig. 7d), which suggest that
266 metal grains could be formed from reduction of Fe-bearing hydrous silicates, and the
267 remnants formed Mg-rich anhydrous silicates as dehydration of hydrous minerals
268 proceeds.
269 (iv) [HS-I to IV] In terms of organic contents, with heating processing, carbon depleted
270 progressively by oxidation to CO/CO_2 based on results of heating experiments using
271 Murchison (Mogi et al., 2017; Nakato et al., 2009; Mogi et al., 2021 submitted).
272 All the mineralogical processes listed above possibly contribute to spectral feature
273 modifications.
274 Laboratory furnace heating experiment of Murchison was performed by Mogi et
275 al. (2017) in order to simulate extensive heating on C-type asteroids due to impacts, solar
276 radiation, and decay of the short-lived radiogenic nuclides. They successfully obtained
277 spectral changes caused by heating as summarized in Table 2 without any adsorbed and
278 rehydrated water effects, and revealed the thermal alteration process and spectral
279 modification occurring at laboratory heating Murchison samples, which is similar to that

at naturally-heated carbonaceous chondrites in this study. Murchison spectra showed darkening toward 400 °C and then brightening up to 900 °C, the 0.7-μm band disappeared at 400 °C, and the 3-μm band became shallower and sharper with peak shift toward shorter wavelength and totally disappeared at 600 °C. These spectral changes directly linked with the mineralogical changes according to XRD analysis results. Hydrous minerals such as serpentine and tochilinite in Murchison, start to decompose and become amorphous at <600 °C, and then secondary anhydrous minerals such as olivine and pyroxene form over 600 °C. This dehydration process is consistent with the result of water content analysis showing water content reduces from 6.8 wt% of unheated Murchison to 0 wt% of 900 °C-heated Murchison (Mogi et al., 2021 submitted).

In this study the 3-μm band of HS-IV and anhydrous sample spectra can be terrestrial water (Fig. 3c). Generally, there is no hydrous phase survived in the HS-IV samples indicated by previous results of XRD analysis (Mogi et al., 2017; Nakamura, 2005; Nakato et al., 2009). For naturally-heated carbonaceous chondrites, heated over 750 °C at their parent bodies, FeNi grains have been distributed (Figs. 6, 7), which indicates that the dehydration process has been completed at HS-IV. For experimentally-heated Murchison reported by Mogi et al. (2017; 2021 submitted), XRD patterns indicated that hydrous minerals completely decompose over 600 °C, and replaced by secondary anhydrous silicates, and at the same time metal grans have started to be formed. Previous XRD and water content analyses revealed that when the experimentally heated sample was once exposed to Earth's atmosphere after heating, it is immediately contaminated by rehydrated water, which released during heating at 400–600 °C, and causes a wide 3-μm band (Mogi et al., 2017; Mogi et al., 2021 submitted). In this study, the 3-μm band at HS-IV samples and Allende survives at up to 400 °C-heated environments, which indicates that rehydrated terrestrial water cannot be easily removed once the rehydration event has occurred. In addition, there could be an effect on spectra by OH-bearing minerals formed by terrestrial weathering such as goethite α-$Fe^{3+}O(OH)$, akaganeite β-$Fe^{3+}O(OH)$, and lepidocrocite γ-$Fe^{3+}O(OH)$ that dehydrated at ~250–300 °C (Naono et al., 1987; Özdemir & Dunlop, 2000). The 3-μm band of all spectra in this study would contain the water absorption bands due to rehydrated water and weathering minerals. The spectral measurements of in-situ heating at 400 °C may not be enough to

311 remove rehydrated water from chondrites which heated over 600 °C at their parent bodies.
312
313 **4.2.1. Albedo change**
314 There is the step-by-step albedo change as heating stage increases as shown in Fig.
315 2a and b. First, amorphization and decomposition of serpentine and tochilinite, both of
316 which have relatively high Vis-IR albedo >10% (Cloutis, Hudon, Hiroi, Gaffey, & Mann,
317 2011), occurs at HS-II and reduces the reflectance of HS-I samples. Second, toward HS-
318 IV, reflectance increasing may occur due to sum of the several competing effects as
319 follows:
320 (a) Formation of olivine and pyroxene, which have high reflectance ~40–80% (Cloutis et
321 al., 2012), caused brightening. CF and RB showing differences of silicate features
322 supporting secondary anhydrous silicates formation at HS-IV (Fig. 5; discussed in detail
323 in section 4.2.3).
324 (b) Fe-enriched metal grains - observed by TEM analysis (Figs. 6b, c, and 7c) would
325 cause spectral darkening based on the result that metal particles >50 nm in diameter cause
326 darkening without reddening reported by Lucey & Noble (2008).
327 (c) Carbon depletion proceeded (from 3.10±0.05 wt% of unheated Murchison to 0.63±
328 0.02 wt% at 900 °C heated sample; Mogi et al., 2017), according to the results
329 experimentally-heating on Murchison meteorite, and caused albedo increasing over
330 600 °C heating (~4 and ~8% at 0.55 μm of 600 and 900 °C heated sample spectra,
331 respectively). It is consistent with the results in this study that albedo increases as heating
332 stage becoming high to HS-IV.
333
334 **4.2.2. 0.7- and 3-μm bands weakening**
335 The progress of amorphization and dehydration of serpentine and tochilinite
336 caused depths decreasing of the 0.7- and 3-μm bands. At the same time, the peak position
337 of the 3-μm band shifts toward shorter wavelength from HS-I to HS-II (Figs. 2, 3, and
338 Table 1). Tochilinite whose peak of the 3-μm band is at ~2.77 μm (Ljuba V. Moroz,
339 Schmidt, Schade, Hiroi, & Ivanova, 2006) decomposed at relatively lower temperature,
340 and then serpentine whose peak of the 3-μm band at ~2.71–2.72 μm (Salisbury, 1991;
341 Beck et al., 2010) decomposed as heating proceeds. Long-duration heating experiments

using Murchison performed by Mogi et al. (2017) and Mogi et al. (2021, submitted) show that the 3-μm band peak shifts by ~0.06 μm until the 3-μm band completely disappear at 600 °C (from ~2.80 μm of unheated Murchison to ~2.74 μm of Murchison heated at 500 °C). After hydrous mineral decomposition finished, the shallow and round 3-μm band with a peak shifted longer wavelength in HS-IV spectra could be due to terrestrial rehydrated water (Fig. 3c).

4.2.3. CF and RB changes

CF of HS-I and II samples presents at almost similar wavelength and also consistent with the previous report by Salisbury et al. (1991), however, Y 980115 and Jbilet Winselwan show a wavelength shift. CF of HS-IV chondrites and Allende is also shifted toward longer wavelength compared with that of HS-I and II samples. We are aware that the wavelength range where CF appears could depend on not only heating stage but the subtype of carbonaceous chondrites as summarized by Salisbury et al. (1991). The RBs exist between ~10–13 μm of each sample spectrum as shown in Fig. 5 as Si-O asymmetric stretching mode (e.g., (Hunt, 1982; Reddy, 2017; Lyon, 1964; McAdam et al., 2015; Salisbury et al., 1991). RB of HS-I and II is almost similar and reflects the existence of hydrous silicates even the silicate becomes amorphous. For HS-IV, RB is significantly different from that of HS-I and II samples, which indicates the formation process of secondary anhydrous minerals which replaced by hydrous silicates starting at HS-II and toward HS-IV. Production of secondary olivine and low-Ca pyroxene at higher heating stage also caused Vis-IR albedo increasing (Figs. 2a, b, and 7c; discussed in detail in section 4.2.1). In the light of serpentine amorphization proceeding from HS-I to HS-II, reflectance spectra show no significant difference in MIR range except for uncharacterized peak at ~10.7 μm (Fig. 5). In order to detect MIR spectral changes due to silicate amorphization in detail, it would be effective to perform transmission spectroscopy which can detect highly-disordered silicates in CM and CI chondrites (Beck et al., 2010, 2014).

4.3. Comparison between long-duration heating and short-duration heating

Naturally-heated chondrites show that, as described above, the 3-μm band

diminished and finally almost disappeared at HS-IV, and Vis-IR slope decreases with increasing heating stage (Fig. 2a and b). In particular, as explained in section 4.1, HS-II and IV spectra measured by in-situ heating at 400 °C show the 3-μm band mainly due to structural water, and less contaminated with terrestrial water compared with those measured by in-situ heating at 120 °C (Figs. 1c–i, 3b, and c).

Due to short-duration heating, in contrast to long-duration heating of a ten-hour-scale heating performed by laboratory experiments and a million-year-scale heating by in-space thermal alteration processes, performed by laser-heating experiments using Murchison meteorite, the 3-μm band depth and Vis-IR slope decrease as laser energy increases (e.g., Matsuoka et al., 2020). The experiment simulated nano-second order heating induced by micrometeoroid bombardments at the surface of the airless small bodies. Comparison of short-duration heating performed by Matsuoka et al. (2015; 2020) with long-duration heating of this study is performed using the 3-μm band strength, which described former in section 4.1, and Vis-IR slope defined as follows:

$$\text{Vis} - \text{IR slope} = \{\text{R}(0.95) - \text{R}(0.39)\}/0.56$$

where R (λ) stands for reflectance at λ μm in wavelength.

Figure 9 exhibits a positive correlation between the 3-μm band depth and Vis-IR spectral slope regarding both laser-heating and natural-heating effects. All laser-irradiated Murchison samples show that the 3-μm band decreases but remains detectable even at the highest irradiation energy 15 mJ. For naturally- and experimentally-heated chondrite samples, the 3-μm band decreases through HS-II and 300–500 °C heating, and almost vanishes at HS-IV and >600 °C heating. While the regression line slope of laser-heated samples is 0.152, the slope of naturally-heated samples is 0.045 (all spectra measured at 120 °C heating) decreasing by ~70% compared to laser-heated samples. In addition, the regression line slope of experimentally heated Murchison is 0.121 which is similar to that of laser-heated Murchison.

The other parameters such as the 3-μm band peak position as shown in Fig. 10 would be distinguishable the alteration due to short-duration local heating from that due to long-duration extensive heating. In the laser-heating experiment, spectral slope decreases continuously as laser energy increases up to 15 mJ, however, the 3-μm band becomes weaker without peak shifts, which apparently differ from the 3-μm band

404 weakening in the furnace heating (Fig. 10).

405 These trends of band-depth and slope decreasing shown in Figs. 9 and 10
406 corresponds to mineralogical changes due to short- and long-duration heating (discussed
407 in section 5 in detail). Amorphization and dehydration of hydrous minerals progress in
408 both heating processes, but finishes incompletely due to short-duration heating. In
409 contrast, dehydration of hydrous minerals finished at HS-IV and 900 °C due to long-
410 duration heating.

411 In Fig. 10, shift of the 3-μm band center is a key. Due to short-duration heating,
412 the 3-μm band peak position is stable in spite of the depth decreases. It would be because
413 hydrous minerals become amorphous and their bulk mineral species and chemical
414 compositions do not change due to short-duration heating. On the contrary, in the case of
415 naturally-heated chondrites, the 3-μm band peak shifts toward shorter wavelength range
416 with depth decreasing, indicating mineral species are changed, i.e., as described in section
417 4.2, until dehydration of hydrous minerals was completed, tochilinite first and then Fe-
418 rich serpentines became amorphous and dehydrated preferentially, and Mg-rich
419 serpentines and a few Fe-rich serpentines dominated. At the asteroid surface, both heating
420 process of short- and long-duration would occur constantly and change reflectance
421 spectra. The detailed are discussed in section 4.4.

422

423 **4.4. Comparison between carbonaceous chondrites and Ryugu surface materials**

424 Based on our laboratory results obtained by FT-IR and TEM/EDX analyses as
425 shown in Table 3, amorphization and decomposition of hydrous minerals will occur
426 commonly by long-duration heating as well as short-duration heating on C-type asteroids.

427 For spectral changes, long-duration heating changes the 3-μm band peak shifted
428 toward shorter wavelength range and decreases the depth, and finally gets rid of the
429 absorption due to completed dehydration. The 0.7-μm band disappears earlier, at HS-II
430 (Mogi et al., 2017; 2021 submitted, and this study). Short-duration heating makes the 3-
431 and 0.7-μm band shallower, but cannot remove them because the dehydration process
432 stays incomplete (Matsuoka et al., 2020, 2015). FeS-rich amorphous silicate grains are
433 formed and deposited at outermost surface by short-duration heating due to such as
434 micrometeoroid bombardments, and FeNi grains are formed inside due to high-

435 temperature long-duration heating as HS-IV.

436 Ryugu spectra show low albedo, weak but sharp absorption band at 2.72 μm, and
437 little 0.7-μm band, being well consistent with moderately heated carbonaceous chondrite
438 properties as suggested by previous studies (e.g., Kitazato et al. 2019; Sugita et al., 2019).
439 It would be possible that moderately-heated Ryugu surface may not contain secondary
440 FeNi grains formed after dehydration completed, but possibly possess the other
441 nanoparticles in sub-micrometer-order surface materials. Recently Tatsumi et al. (2021,
442 submitted) reveals that at north and south pole regions and northern area of Ryugu show
443 the 0.7-μm absorption band, thus, Ryugu may partly preserve unheated and Fe^{2+}- and
444 Fe^{3+}-bearing carbonaceous materials similar to HS-I CM samples at the surface. In
445 addition, exogenic materials on Ryugu have been also detected such as S-type-like
446 boulders (Tatsumi et al., 2020; Sugimoto et al. 2021, in revision). Hayabusa2's returned
447 samples have been collected twice around the equatorial ridge, from touchdown (TD) 1,
448 and after the impact experiment from TD2 sites. Thus, two types of Ryugu materials, i.e.,
449 of different degrees of space weathering, would be expected to be analyzed, and possibly
450 contain pole-region materials and/or exogenic materials. It is expected that sample
451 analyses will clarify the origin and heating process of Ryugu, direct connection to
452 laboratory meteorites and observed asteroids, and furthermore space weathering effects
453 on preheated carbon/water-bearing materials at the asteroidal surface.
454

455 ## 5. Conclusion

456 The reflectance spectra of naturally-heated carbonaceous chondrites show 3-μm
457 band depth decreasing, albedo and spectral slope changes, and CF and RB changes with
458 increasing heating degree. TEM/EDX observation revealed that Fe- and Ni-rich small
459 metal grains smaller than 1 μm in diameter distribute over the interior of severely heated
460 chondrites. The secondary anhydrous silicates were also observed in the strongly heated
461 chondrites. In proportion to the heating degree, amorphization and dehydration of
462 serpentine and tochilinite from HS-I to HS-II may cause the 0.7- and 3-μm band
463 weakening, spectral slope decreasing, and albedo decreasing of chondrite spectra. In
464 addition, formation of secondary olivine, pyroxene, and FeNi-rich metal grains at HS-IV
465 would be responsible for the 3-μm band depth decreasing, spectral slope increasing,

albedo increasing, CF peak shift, and RB changes of chondrite spectra. Those spectral changes in response to mineralogical alteration processes will be useful to interpret in-space target surface composition by ground-based and/or remote-sensing observation.

Acknowledgements

This study was supported by Japan Society for the Promotion of Science (JSPS) Core-to-Core program "International Network of Planetary Sciences", JSPS Japanese–German Graduate Externship, and KAKENHI from JSPS Grant-in-Aid for Scientific Research on Innovative Areas (Aqua Planetology, grant No. JP17H06459). The Focused Ion Beam (FEI, Scios DualBeam) and the TEM (FEI, Titan G2 S/TEM) at Bayerisches Geoinstitut were financed by a DFG grant No. INST 91/315-1 FUGG and No. INST 91/251-1 FUGG, respectively.

Figures

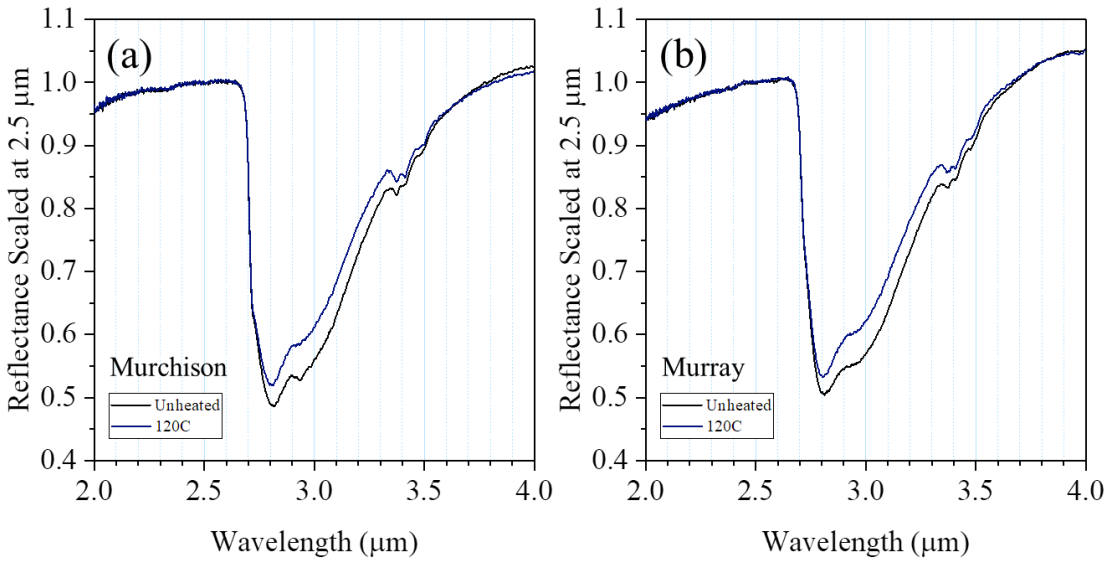
(a)
Murchison
Unheated
120C
Reflectance Scaled at 2.5 µm
Wavelength (µm)
(b)
Murray
Unheated
120C
Reflectance Scaled at 2.5 µm
Wavelength (µm)

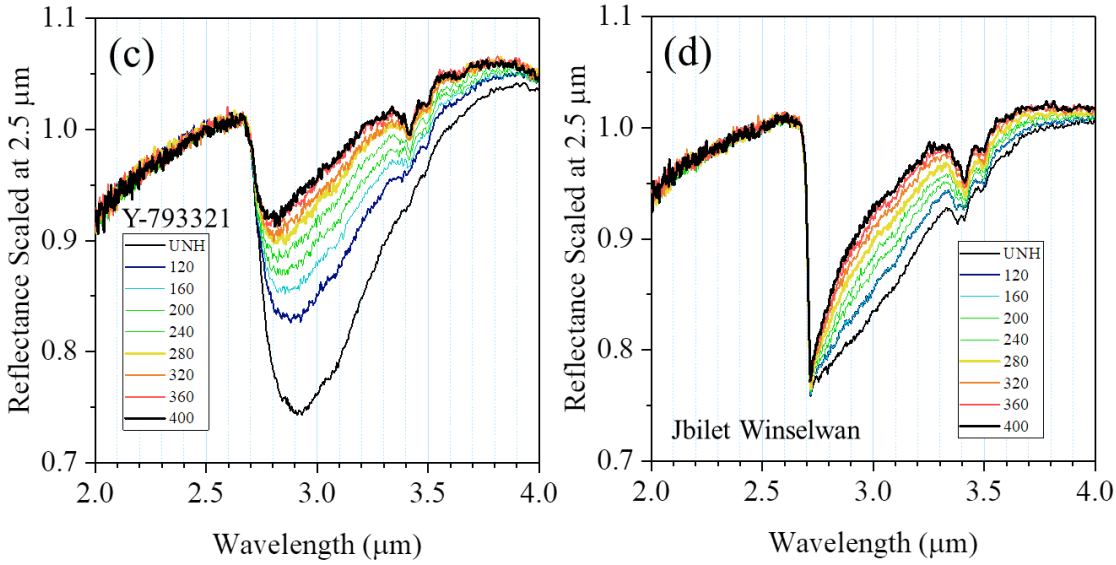
(c)
Y-793321
UNH
120
160
200
240
280
320
360
400
Reflectance Scaled at 2.5 µm
Wavelength (µm)
(d)
Jbilet Winselwan
UNH
120
160
200
240
280
320
360
400
Reflectance Scaled at 2.5 µm
Wavelength (µm)

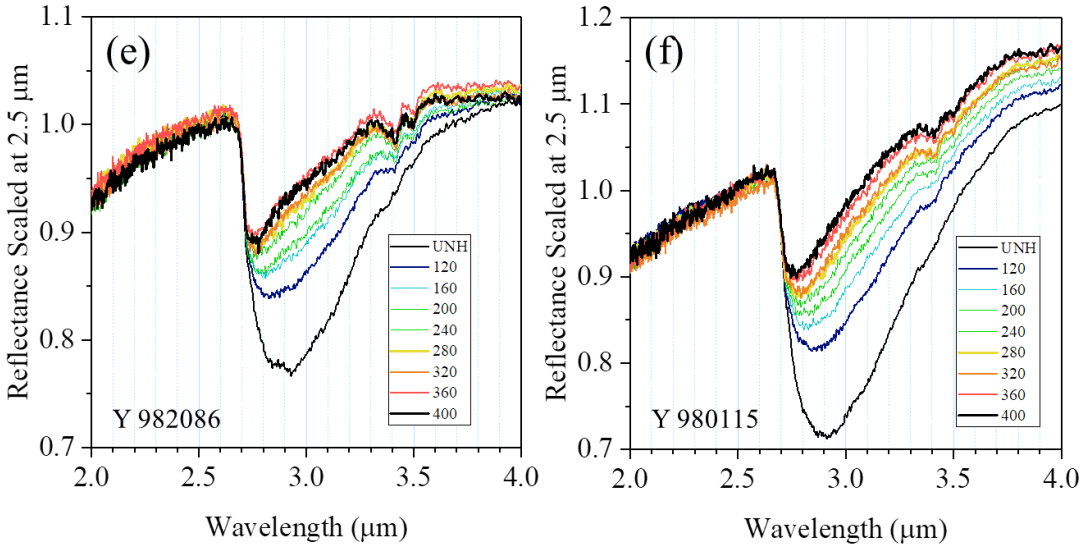
(e)
Y 982086
UNH
120
160
200
240
280
320
360
400
Reflectance Scaled at 2.5 µm
Wavelength (µm)
(f)
Y 980115
UNH
120
160
200
240
280
320
360
400
Reflectance Scaled at 2.5 µm
Wavelength (µm)

482

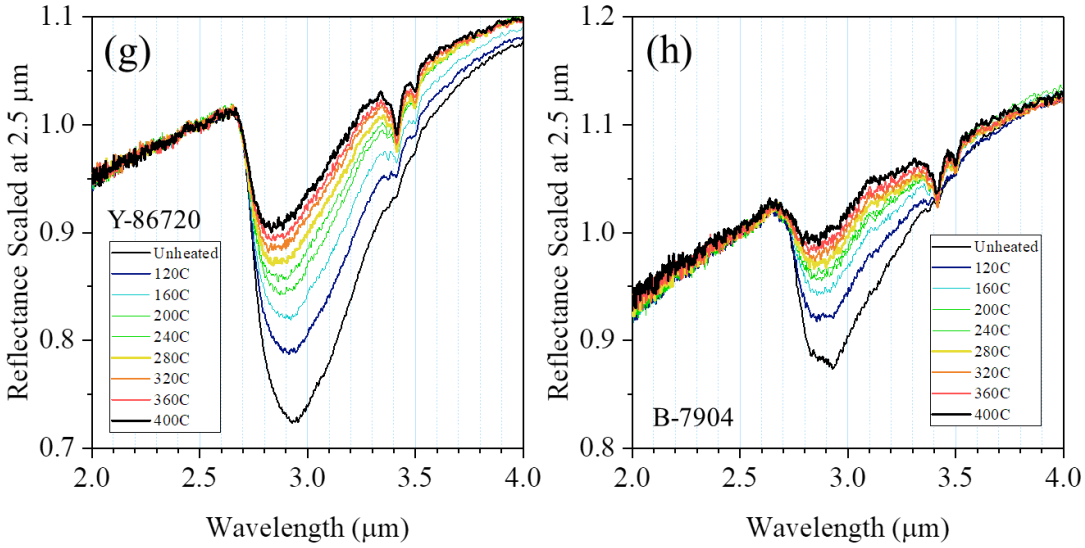
(g)
Y-86720
Unheated
120C
160C
200C
240C
280C
320C
360C
400C
Reflectance Scaled at 2.5 µm
Wavelength (µm)
(h)
B-7904
Unheated
120C
160C
200C
240C
280C
320C
360C
400C
Reflectance Scaled at 2.5 µm
Wavelength (µm)

483

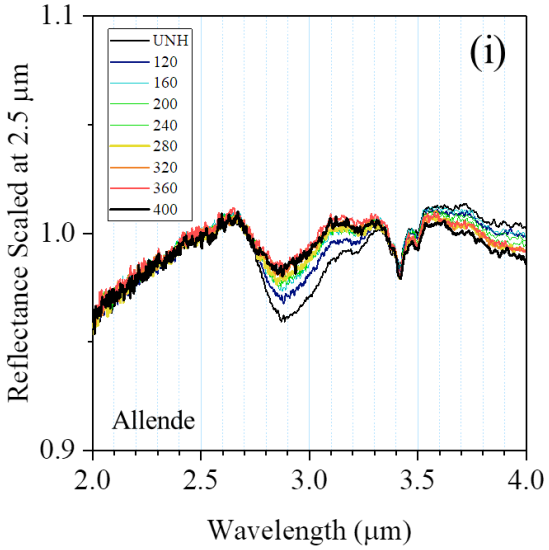
(i)
Allende
UNH
120
160
200
240
280
320
360
400
Reflectance Scaled at 2.5 µm
Wavelength (µm)

484

485 Fig. 1. IR spectra of Y-793321 measured at different temperatures from room temperature
486 to 400 °C of Murchison (a), Murray (b), Y-793321 (c), Jbilet Winselwan (d), Y 982086
487 (e), Y 980115 (f), Y-86720 (g), B-7904 (h), and Allende (i). The absorption bands consist
488 of adsorbed and interlayer water (Beck, Pommerol, et al., 2010), however, adsorbed water
489 is removed due to heating. Spectra are scaled at 2.5 μm for clarify. "UNH" = unheated,
490 and "120" – "400" = heated at 120–400 °C.

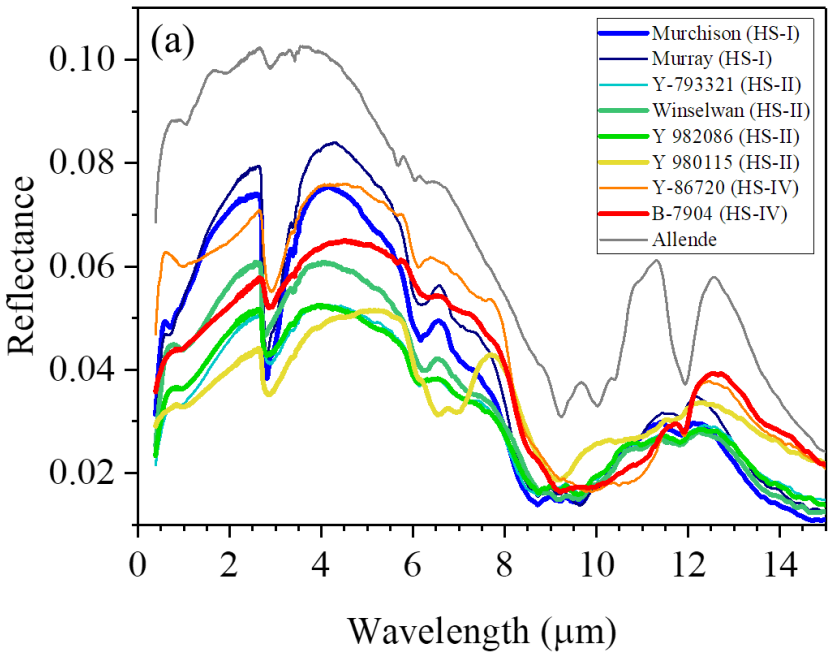

491

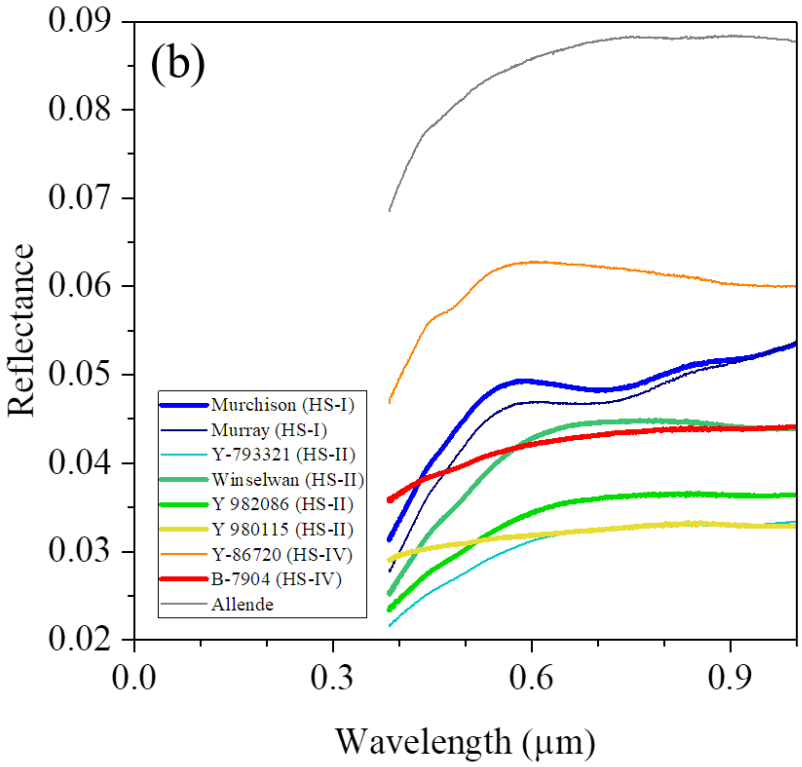

492

493 Fig. 2. Vis-IR reflectance spectra in 0.38–15 μm (a) and 0.38–1 μm (b). Albedo of HS-II
494 samples are lower compared with HS-I and HS-IV samples. The 0.7-μm absorption band
495 is detectable in HS-I spectra.

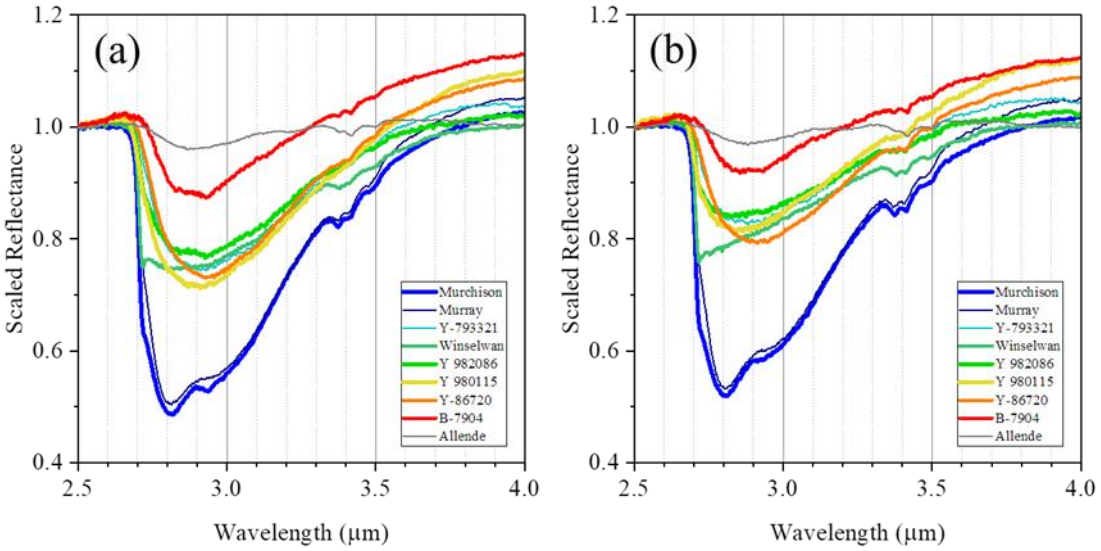

496

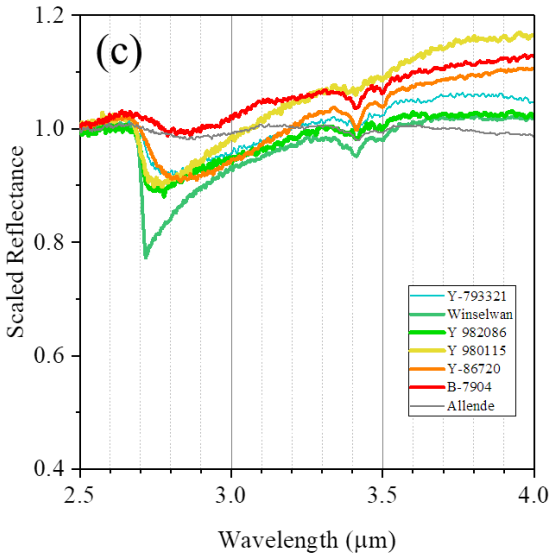

497

498 Fig. 3. Reflectance spectra scaled at 2.5 μm of chondrite samples. The 3-μm band
499 measured at room temperature (a) changes sharp and shallow due to in-situ heating at
500 120 °C (b) and 400 °C (c).

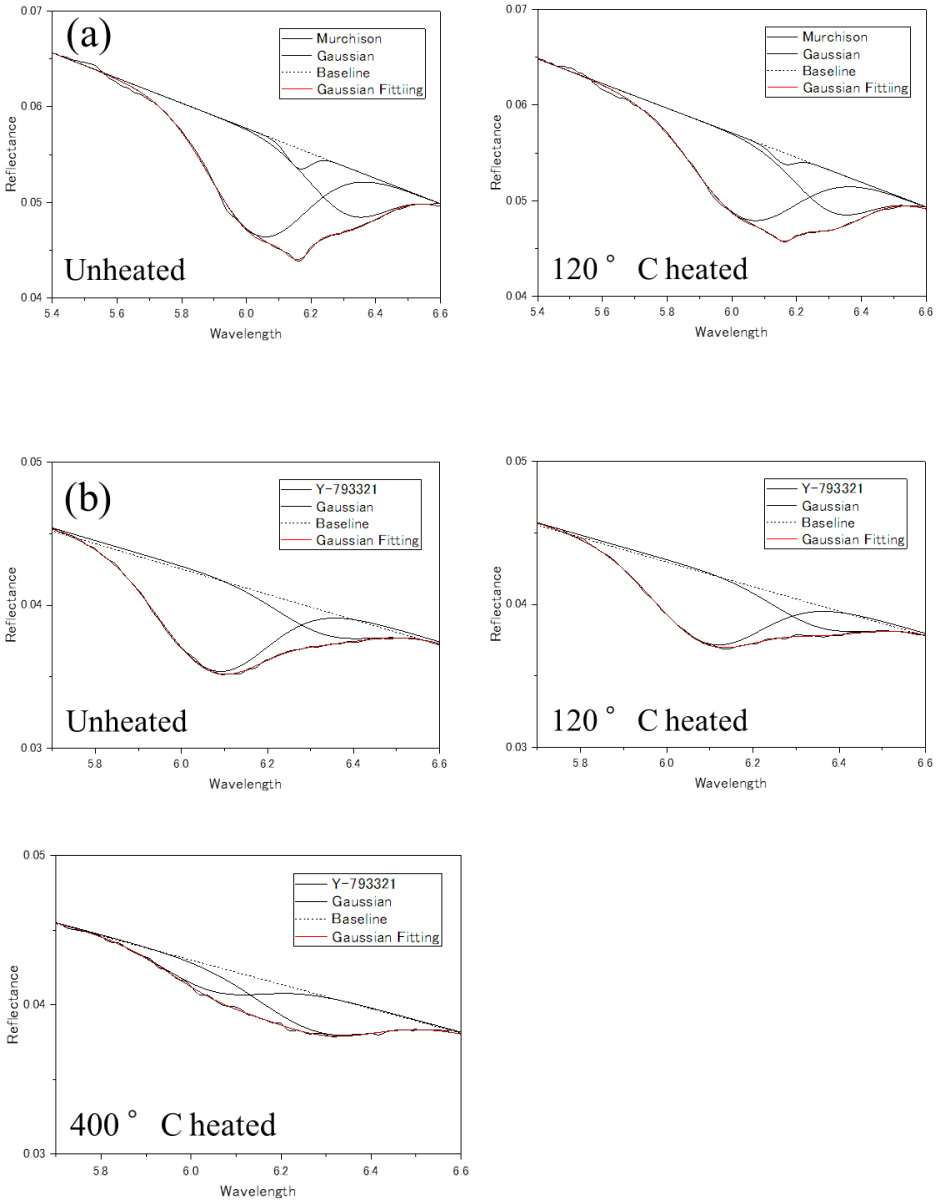

Fig. 4. Reflectance spectra of chondrite samples over the range of 5.4–6.6 μm. Murchison spectra shows an unique peak at ~6.16 μm, which survives heating up to 120 °C (a). Y-793321 spectra show depth decreasing with heating degree increasing up to 400 °C (b).

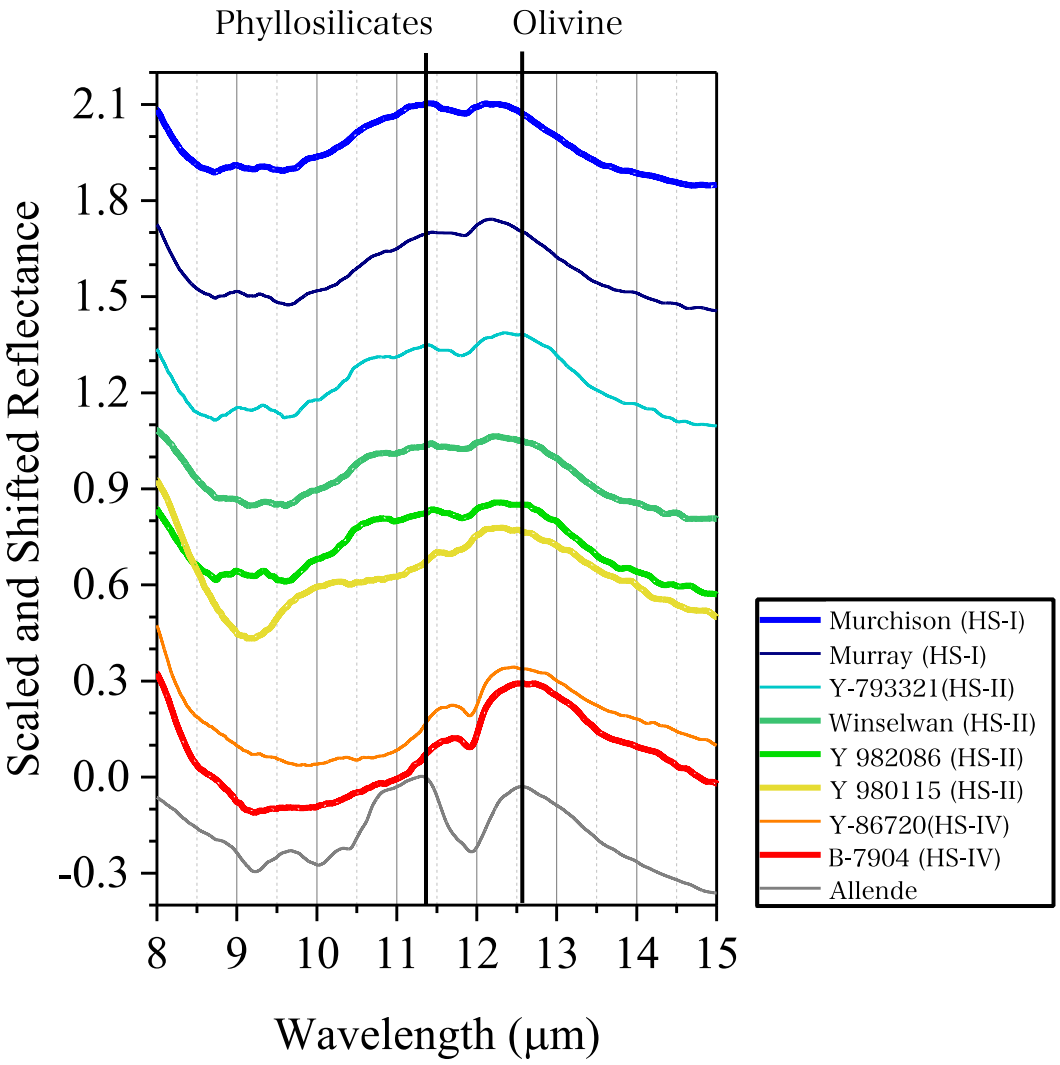

510

511 Fig. 5. Scaled and shifted MIR spectra of chondrites. HS-I and II spectra are similar but
512 HS-IV show CF shift and olivine features at RB. Y 980115 and Allende have different
513 spectral shapes (e.g., around CF) compared with the other chondrites.

514

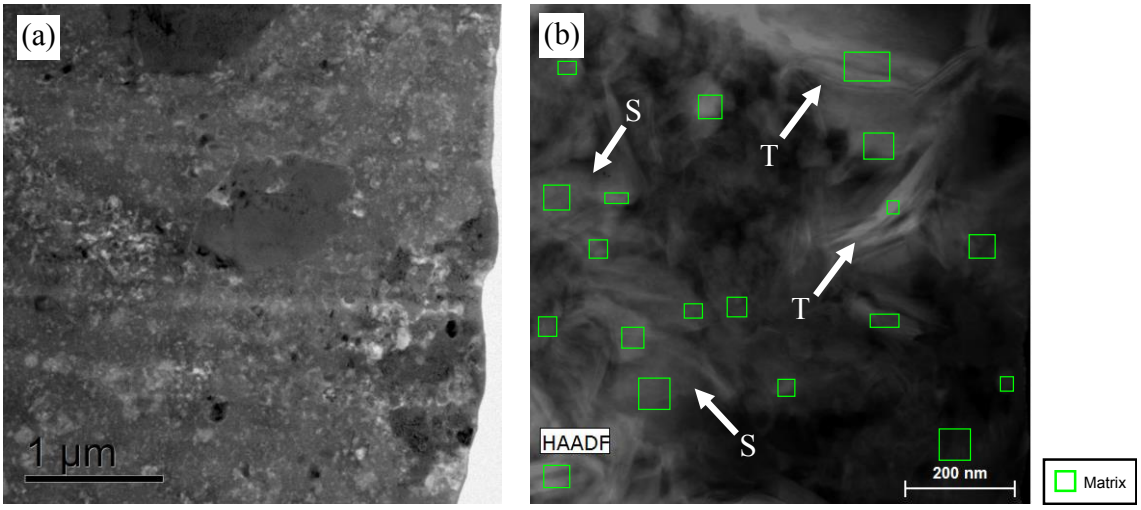

515

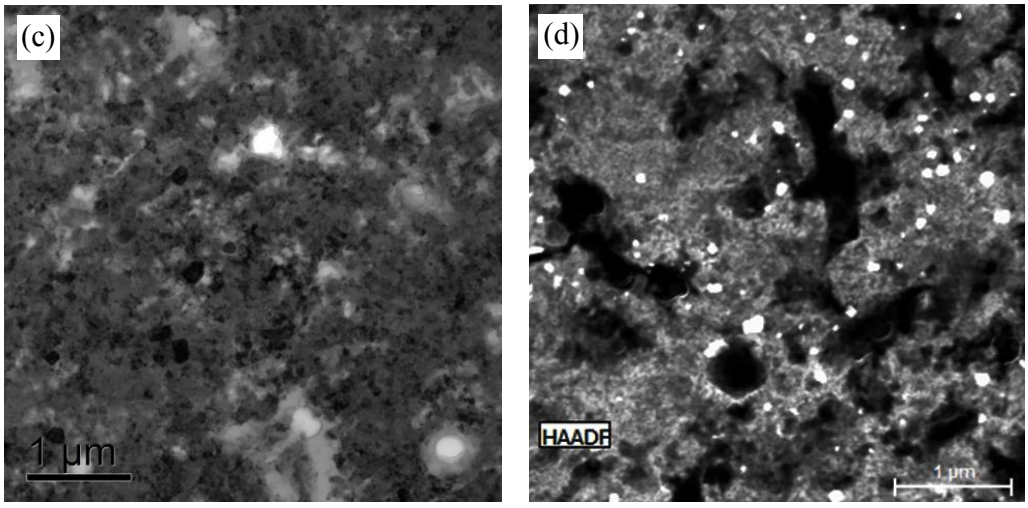

516

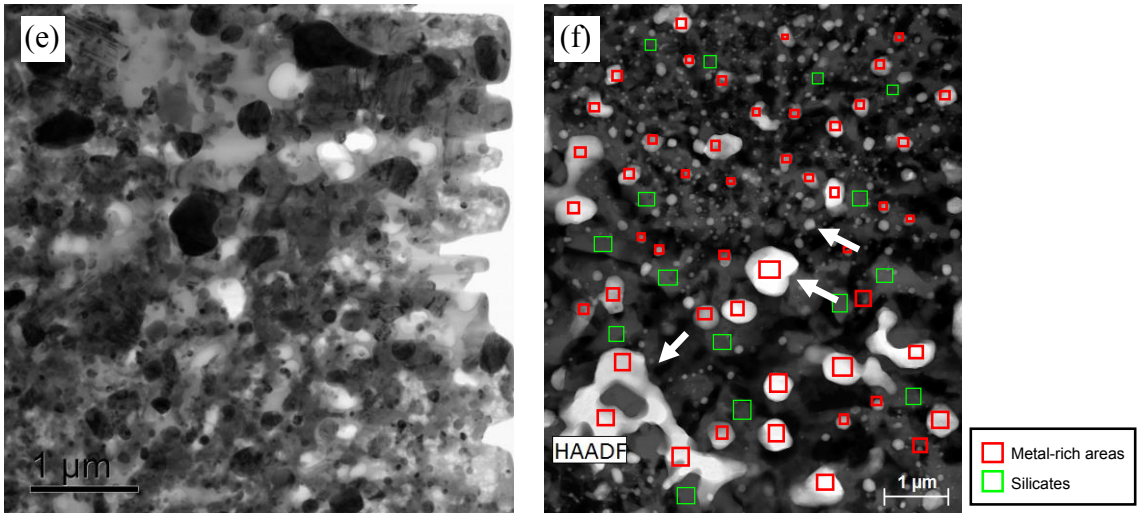

517

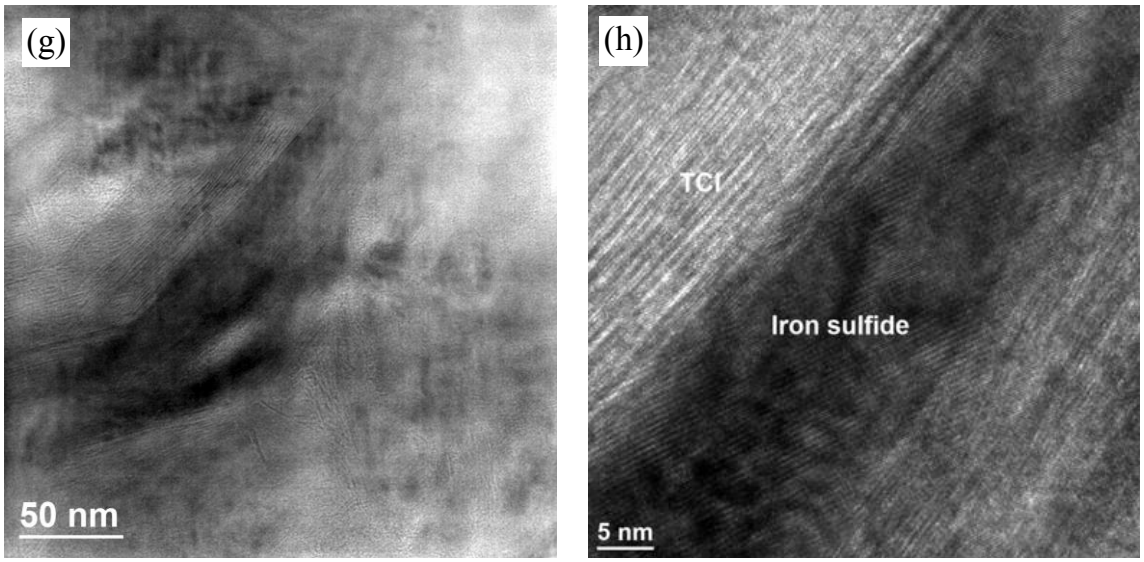

518

519 Fig. 6. Bright field (BF) TEM image (a) and bright field STEM image (b) of matrix TCI
520 in LEW87022, and BF-TEM and HAADF-STEM images of matrices in Dhofar 735 (c,
521 d) and Murchison heated at 900 °C (e, f). BF-STEM images of matrix TCI in
522 LEW87022 (b) showing fibrous structure indicates tochilinite "T" and serpentine "S",
523 and matrices in Dhofar 735 (d) and Murchison heated at 900 °C (f). Small grains
524 (<1000 nm) observed the entire region of FIB sections as indicated by arrows in Fig. 6f.
525 Squares are the selected areas of EDX analyses (See Fig. 7). The HRTEM images of
526 TCI and the FeS-rich grain in the map area (g), indicated by the lower T-labeled
527 arrowhead in the Fig. 6b, and of TCI (upper) and iron sulfide (center) (h).

528

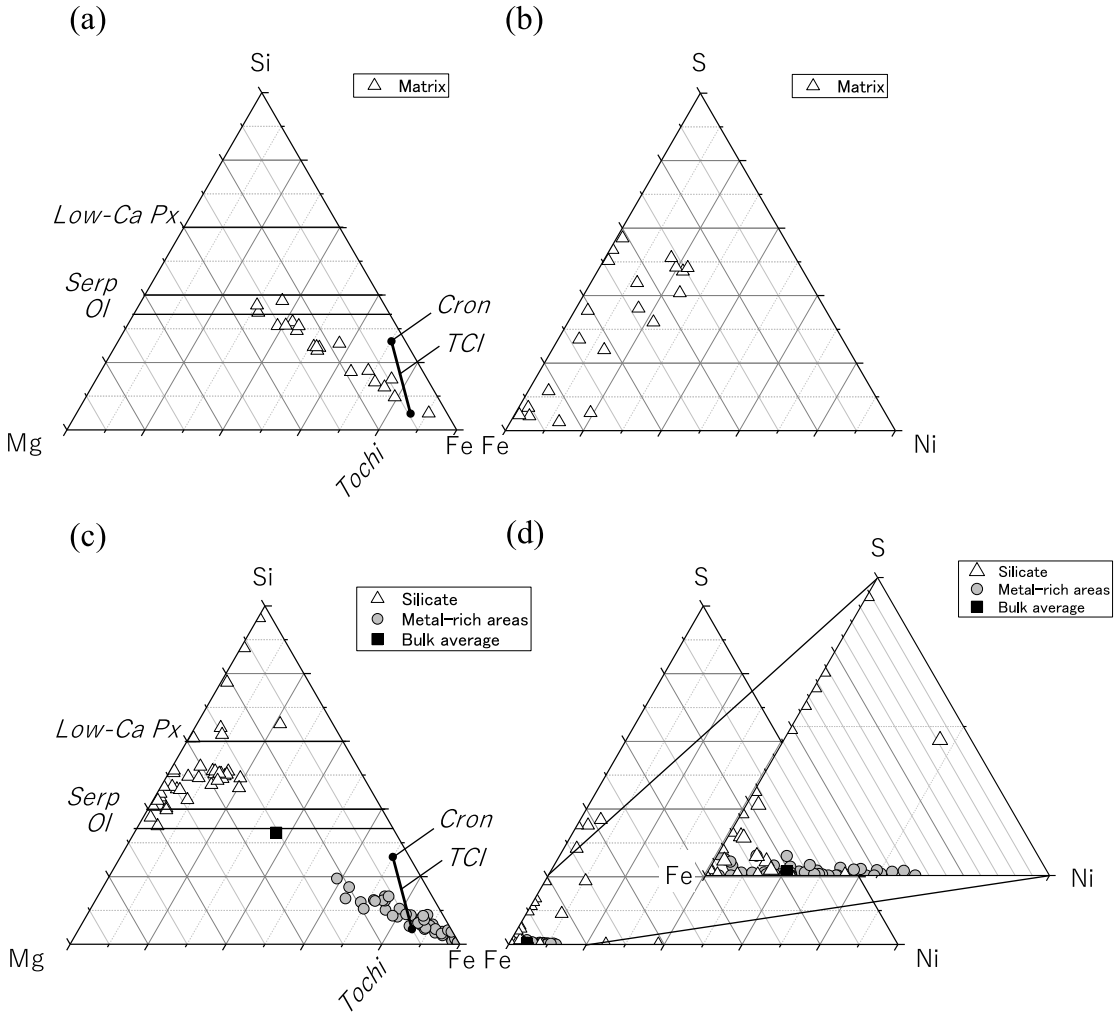

529

530 Fig. 7. Ternary plots of Si-Mg-Fe and S-Fe-Ni systems of atomic ratios from STEM-EDX
531 analysis. The elemental ratios of the matrix minerals in LEW87022 show a wide range of
532 the elemental ratios of Si-Mg-Fe (a) and S-Fe-Ni (b), however, those of matrix minerals
533 in Murchison heated at heated at 900 °C show a binary cluster of Fe-poor silicate and Fe-
534 rich metal grains (c). Sulfur is extremely depleted in metal grains of Murchison heated at
535 heated at 900 °C (d). Abbreviations; serpentine (Serp), olivine (Ol), pyroxene (Px),
536 cronstedtite (Cron), and tochilinite (Tochi).

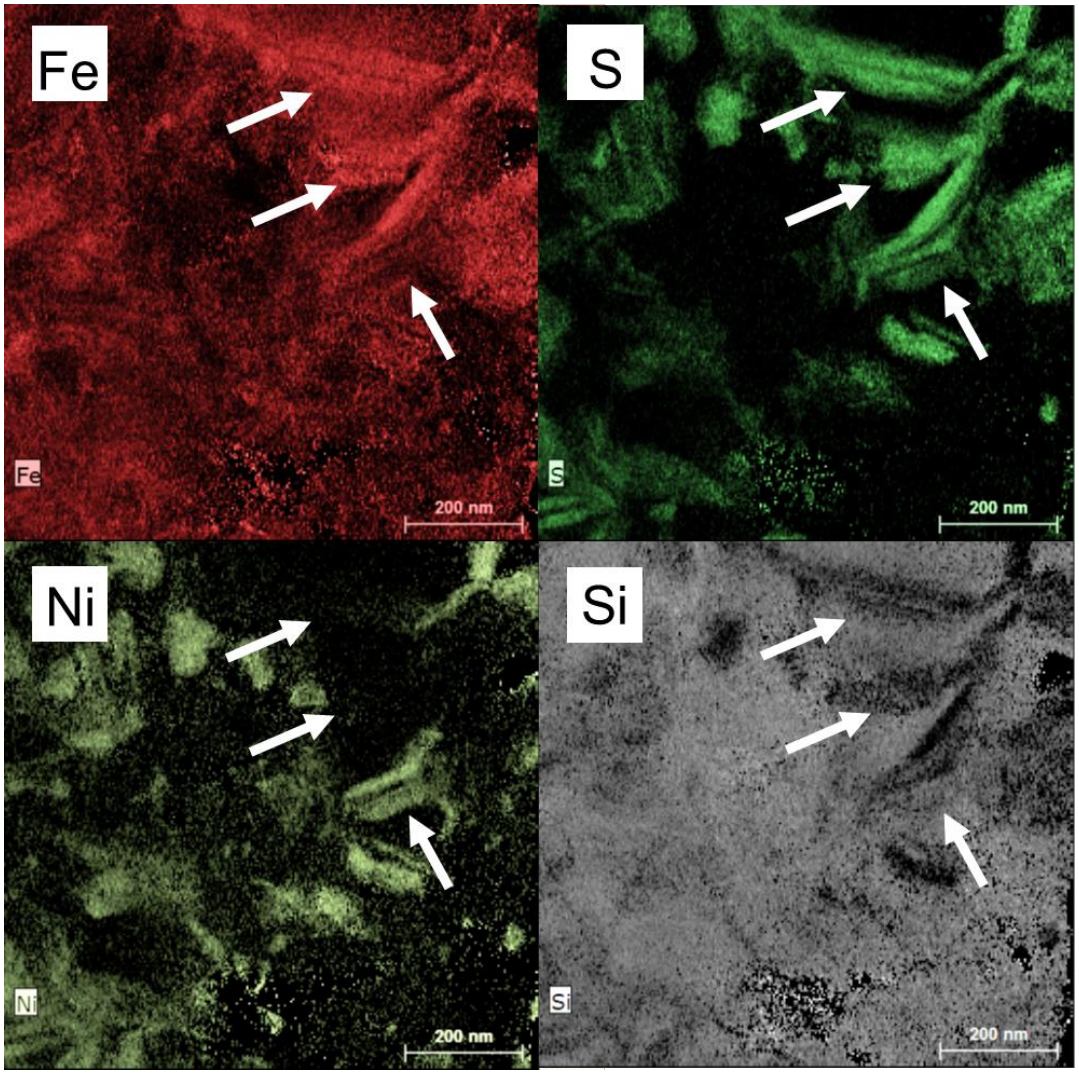

Fig. 8. TEM-EDX elemental distribution maps of TCI in LEW87022 as same region shown in Fig. 6a. FeS-rich grains indicated by arrows show different Ni contents.

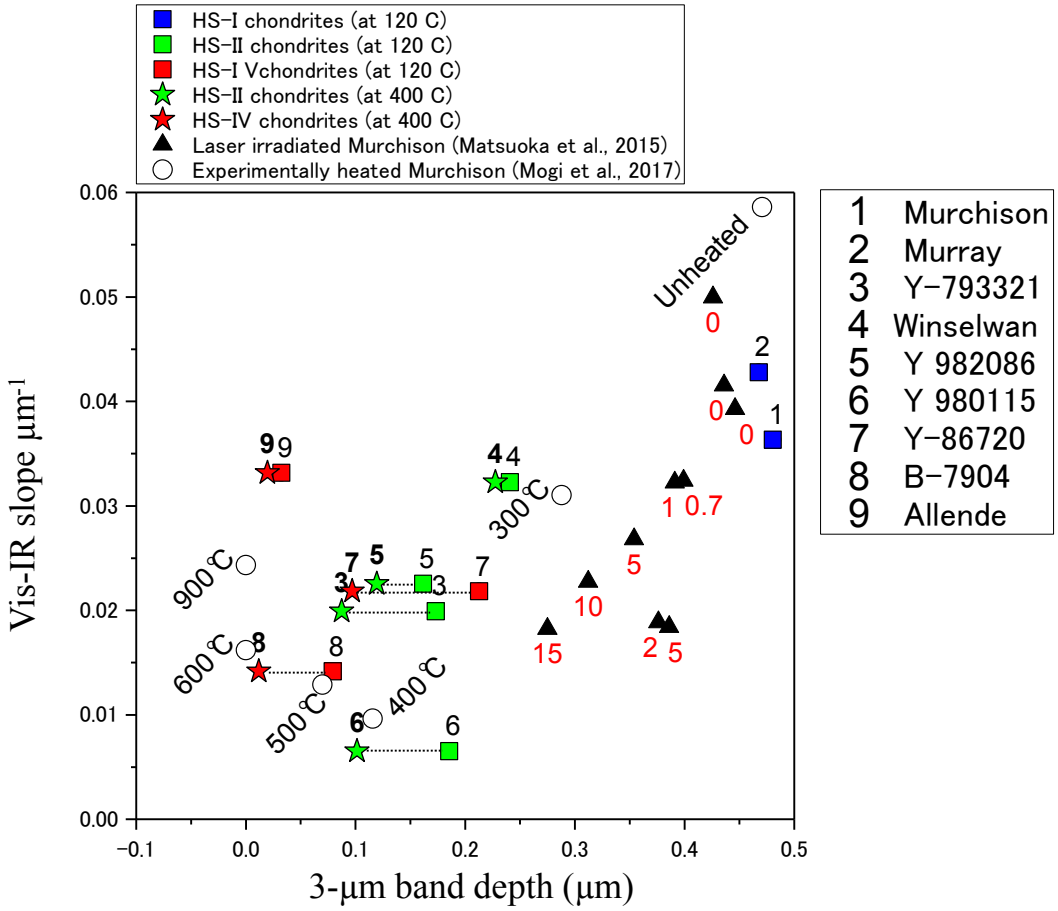

541

542

543 Fig. 9. Relationship between the 3-μm band depth and spectral slope over the 0.39–0.95
544 μm in wavelength. Sample points of "Unheated", "300 °C", "400 °C", …, "900 °C", and
545 "0", "0.7", "1", …, "15" (red numbers) stand for experimentally-heated samples of
546 furnace and laser heating, respectively. Sample points of "1", "2", "3", …, "9" (black
547 numbers) stand for naturally-heated samples. Labels: 1 = Murchison, 2 = Murray, 3 = Y-
548 793321, 4 = Jbilet Winselwan, 5 = Y 982086, 6 = Y 980115, 7 = Y-86720, 8 = B-7904,
549 and 9 = Allende.

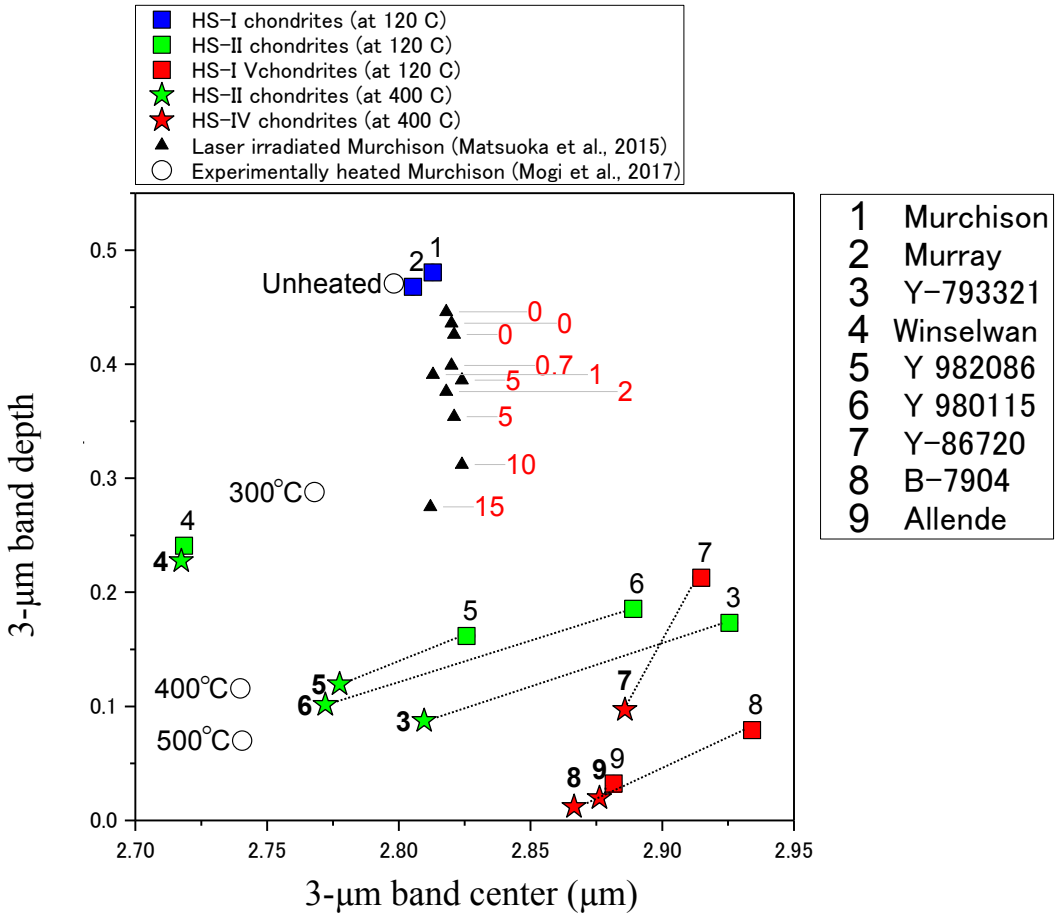

Fig. 10. Relationship between the 3-µm band center wavelength and depth. Sample points of "Unheated", "300 °C", "400 °C", "500 °C", and "0", "0.7", "1", …, "15" (red numbers) stand for experimentally-heated samples of furnace and laser heating, respectively. Sample points of "1", "2", "3", …, "9" (black numbers) stand for naturally-heated samples. Labels: 1 = Murchison, 2 = Murray, 3 = Y-793321, 4 = Jbilet Winselwan, 5 = Y 982086, 6 = Y 980115, 7 = Y-86720, 8 = B-7904, and 9 = Allende.

Tables (Caption)

Table 1. The band centers, depths, reflectances, and slopes of chondrite spectra.

Table 2. Summary of mineralogical and spectral changes of Murchison samples experimentally heated at 300, 400, 500, 600, and 900 °C reported by Mogi et al. (2017).

Table 3. Summary of mineralogical and spectral changes of carbonaceous chondrite due to short- and long-duration heating events.

References

Akai, J. (1992). T-T-T diagram of serpentine and saponite, and estimation ofmetamorphic heating degree of Antarctic carbonaceous chondrites, *5*, 120–135.

Beck, P., Garenne, A., Quirico, E., Bonal, L., Montes-Hernandez, G., Moynier, F., & Schmitt, B. (2014). Transmission infrared spectra (2-25μm) of carbonaceous chondrites (CI, CM, CV-CK, CR, C2 ungrouped): Mineralogy, water, and asteroidal processes. *Icarus*, *229*, 263–277. https://doi.org/10.1016/j.icarus.2013.10.019

Beck, P., Pommerol, A., Schmitt, B., & Brissaud, O. (2010). Kinetics of water adsorption on minerals and the breathing of the Martian regolith. *Journal of Geophysical Research E: Planets*, *115*(10), 1–11. https://doi.org/10.1029/2009JE003539

Beck, P., Quirico, E., Montes-Hernandez, G., Bonal, L., Bollard, J., Orthous-Daunay, F. R., … Guillot, S. (2010). Hydrous mineralogy of CM and CI chondrites from infrared spectroscopy and their relationship with low albedo asteroids. *Geochimica et Cosmochimica Acta*, *74*(16), 4881–4892. https://doi.org/10.1016/j.gca.2010.05.020

Berlanga, G., Hibbitts, C. A., Takir, D., Dyar, M. D., & Sklute, E. (2016). Spectral nature of CO2 adsorption onto meteorites. *Icarus*, *280*, 366–377. https://doi.org/10.1016/j.icarus.2016.06.020

Bland, P. A., Cressey, G., & Menzies, O. N. (2004). Modal mineralogy of carbonaceous chondrites by X-ray diffraction and Mössbauer spectroscopy. *Meteoritics & Planetary Science*, *39*(1), 3–16. https://doi.org/10.1111/j.1945-5100.2004.tb00046.x

Burbine, T., McCoy, T., Meibom, a, Gladman, B., & Keil, K. (2002). Meteoritic parent bodies: Their number and identification. *Asteroids III*, *1*, 653–667. Retrieved from http://www.mtholyoke.edu/courses/tburbine/tomburbine/burbine.chapter.2002.pdf %5Cnhttp://www.mtholyoke.edu/~tburbine/Burbine.asteroidsIII.20002.pdf

Caillère, S., & Hènin, S. (1957). The chlorite and serpentine minerals. In R. C. Mackenzie (Ed.), *The Differential Thermal Investigation of Clays*. Mineralogical Society, London.

Chen, M., Jiang, J., Zhou, X., & Diao, G. (2008). Preparation of Akaganeite Nanorods and Their Transformation to Sphere Shape Hematite. *Journal of Nanoscience and Nanotechnology*, *8*, 3942–3948. https://doi.org/10.1166/jnn.2008.189

Cloutis, E. A., Hudon, P., Hiroi, T., & Gaffey, M. J. (2012). Spectral reflectance properties of carbonaceous chondrites: 3. CR chondrites. *Icarus*, *217*(1), 389–407. https://doi.org/10.1016/j.icarus.2011.11.004

Cloutis, E. A., Hudon, P., Hiroi, T., Gaffey, M. J., & Mann, P. (2011). Spectral reflectance properties of carbonaceous chondrites: 2. CM chondrites. *Icarus*, *216*(1), 309–346.

https://doi.org/10.1016/j.icarus.2011.09.009
Cloutis, E. A., Hudon, P., Hiroi, T., Gaffey, M. J., Mann, P., & Bell, J. F. (2012). Spectral reflectance properties of carbonaceous chondrites: 3. CR chondrites. *Icarus*, *217*(1), 328–358. https://doi.org/10.1016/j.icarus.2011.11.004
Cloutis, E. A., McCormack, K. A., Bell, J. F., Hendrix, A. R., Bailey, D. T., Craig, M. A., … Riner, M. A. (2008). Ultraviolet spectral reflectance properties of common planetary minerals. *Icarus*, *197*(1), 321–347. https://doi.org/10.1016/j.icarus.2008.04.018
Cudennec, Y., & Lecerf, A. (2005). Topotactic transformations of goethite and lepidocrocite into hematite and maghemite. *Solid State Sciences*, *7*(5), 520–529. https://doi.org/10.1016/j.solidstatesciences.2005.02.002
Duley, W. W., & Lazarev, S. (2004). Ultraviolet Absorption in Amorphous Carbons: Polycyclic Aromatic Hydrocarbons and the 2175 Å Extinction Feature. *The Astrophysical Journal*, *612*(1), L33–L35. https://doi.org/10.1086/424660
Hiroi, T., Pieters, C. M., Zolensky, M. E., & Lipschutz, M. E. (1993). Evidence of thermal metamorphism on the C, G, B, and F asteroids, (5), 5–7.
Hiroi, T., Pieters, C. M., Zolensky, M. E., & Lipschutz, M. E. (1996). Thermal metamorphism of the C, G, B, and F asteroids seen from the 0.7-μm, 3-μm, and UV absorption strengths in comparison with carbonaceous chondrites. *Meteorit Planet Sci*, *31*, 321–327. https://doi.org/10.1111/j.1945-5100.1996.tb02068.x
Hunt, G. R. (1982). Spectroscopic properties of rocks and minerals. In R. S. Carmichael (Ed.), *Handbook of Physical properties of rocks, Volume I* (pp. 295–385). CRC Press. Retrieved from https://www.crcpress.com/Handbook-of-Physical-Properties-of-Rocks-1982-Volume-I/Carmichael/p/book/9781138506794
Ivanova, M. A., Nazarov, M. A., Brandstaetter, F., Moroz, L. V, Ntaflos, T., & Kurat, G. (2005). MINERALOGICAL DIFFERENCES BETWEEN METAMORPHOSED AND NON-METAMORPHOSED CM CHONDRITES.
Jarosewich, E. (1990). Chemical analyses of meteorites: A compilation of stony and iron meteorite analyses. *Meteoritics*, *25*(4), 323–337. https://doi.org/10.1111/j.1945-5100.1990.tb00717.x
Kitazato, K., Milliken, R. E., Iwata, T., Abe, M., Ohtake, M., Matsuura, S., … Tsuda, Y. (2019a). The surface composition of asteroid 162173 Ryugu from Hayabusa2 near-infrared spectroscopy. *Science*, *364*(6437), 272–275. https://doi.org/10.1126/science.aav7432
Kitazato, K., Milliken, R. E., Iwata, T., Abe, M., Ohtake, M., Matsuura, S., … Tsuda, Y. (2019b). The surface composition of asteroid 162173 Ryugu from Hayabusa2 near-

infrared spectroscopy. *Science*. https://doi.org/10.1126/science.aav7432

Lakshmi Reddy, S. (2017). Infrared Spectra in Oxide Nanocomposites/Minerals. In *Correlated Functional Oxides* (pp. 117–138). Cham: Springer International Publishing. https://doi.org/10.1007/978-3-319-43779-8_5

Lantz, C., Clark, B. E., Barucci, M. a., & Lauretta, D. S. (2013). Evidence for the effects of space weathering spectral signatures on low albedo asteroids. *Astronomy & Astrophysics*, *554*, A138. https://doi.org/10.1051/0004-6361/201321593

Lucey, P. G., & Noble, S. K. (2008). Experimental test of a radiative transfer model of the optical effects of space weathering. *Icarus*, *197*(1), 348–353. https://doi.org/10.1016/j.icarus.2008.05.008

Lyon, R. J. P. (n.d.). *Evaluation of infrared spectrophotometry for compositional analysis of lunar and planetary soils /*. Retrieved from http://hdl.handle.net/2027/uc1.b5041254

Ma, C., & Rossman, G. R. (2009). Grossmanite, CaTi 3+ AlSiO 6 , a new pyroxene from the Allende meteorite. *American Mineralogist*, *94*, 1491–1494. https://doi.org/10.2138/am.2009.3310

Matsuoka, M., Nakamura, T., Hiroi, T., Okumura, S., & Sasaki, S. (2020). Space Weathering Simulation with Low-energy Laser Irradiation of Murchison CM Chondrite for Reproducing Micrometeoroid Bombardments on C-type Asteroids. *The Astrophysical Journal*, *890*(2), L23. https://doi.org/10.3847/2041-8213/ab72a4

Matsuoka, M., Nakamura, T., Kimura, Y., Hiroi, T., Nakamura, R., Okumura, S., & Sasaki, S. (2015). Pulse-laser irradiation experiments of Murchison CM2 chondrite for reproducing space weathering on C-type asteroids. *Icarus*, *254*, 135–143. https://doi.org/10.1016/j.icarus.2015.02.029

McAdam, M. M., Sunshine, J. M., Howard, K. T., & McCoy, T. M. (2015). Aqueous alteration on asteroids: Linking the mineralogy and spectroscopy of CM and CI chondrites. *Icarus*, *245*, 320–332. https://doi.org/10.1016/j.icarus.2014.09.041

Mogi, K., Yamashita, S., Nakamura, T., Matsuoka, M., Okumura, S., & Furukawa, Y. (2017). Dehydration process of experimentally heated Murchison without any effects of adsorbed and rehydrated water. In *Annual Meeting of the Meteoritical Society* (Vol. 80, p. 6225).

Morota, T., Sugita, S., Cho, Y., Kanamaru, M., Tatsumi, E., Sakatani, N., … Tsuda, Y. (2020). Sample collection from asteroid (162173) Ryugu by Hayabusa2: Implications for surface evolution. *Science*, *368*(6491), 654–659. https://doi.org/10.1126/science.aaz6306

Moroz, Lyuba, Baratta, G., Strazzulla, G., Starukhina, L., Dotto, E., Barucci, M. A., …

672 Distefano, E. (2004). Optical alteration of complex organics induced by ion
673 irradiation: 1. Laboratory experiments suggest unusual space weathering trend.
674 *Icarus*, *170*(1), 214–228. https://doi.org/10.1016/j.icarus.2004.02.003
675 Moroz, Ljuba V., Schmidt, M., Schade, U., Hiroi, T., & Ivanova, M. A. (2006).
676 Synchrotron-based infrared microspectroscopy as a useful tool to study hydration
677 states of meteorite constituents. *Meteoritics and Planetary Science*, *41*(8), 1219–
678 1230. https://doi.org/10.1111/j.1945-5100.2006.tb00517.x
679 Nakamura, T. (2005). Post-hydration thermal metamorphism of carbonaceous chondrites.
680 *Journal of Mineralogical and Petrological Sciences*, *100*(6), 260–272.
681 https://doi.org/10.2465/jmps.100.260
682 Nakato, A., Nakamura, T., & Noguchi, T. (2009). Mineralogical and chemical variations
683 recorded in dehydrated carbonaceous chondrites. In *72nd Annual Meteoritical*
684 *Society Meeting* (p. 5336). Retrieved from
685 www.lpi.usra.edu/meetings/metsoc2009/pdf/5336.pdf
686 Naono, H., Nakai, K., Sueyoshi, T., & Yagi, H. (1987). Porous texture in hematite derived
687 from goethite: Mechanism of thermal decomposition of geothite. *Journal of Colloid*
688 *And Interface Science*, *120*(2), 439–450. https://doi.org/10.1016/0021-
689 9797(87)90370-5
690 Özdemir, Ö., & Dunlop, D. J. (2000). Intermediate magnetite formation during
691 dehydration of goethite. *Earth and Planetary Science Letters*, *177*(1–2), 59–67.
692 https://doi.org/10.1016/S0012-821X(00)00032-7
693 Ryskin, Y. I. (1974). The Vibrations of Protons in Minerals: hydroxyl, water and
694 ammonium. In *The infrared spectra of minerals* (pp. 137–181).
695 https://doi.org/https://doi.org/10.1180/mono-4.9
696 Salisbury, J. W., D'Aria, D. M., & Jarosewich, E. (1991). Midinfrared (2.5-13.5 μm)
697 reflectance spectra of powdered stony meteorites. *Icarus*.
698 https://doi.org/10.1016/0019-1035(91)90052-U
699 Sugita, S., Honda, R., Morota, T., Kameda, S., Sawada, H., Tatsumi, E., … Tsuda, Y.
700 (2019). The geomorphology, color, and thermal properties of Ryugu: Implications
701 for parent-body processes. *Science*, *364*(6437).
702 https://doi.org/10.1126/science.aaw0422
703 Takir, D., Emery, J. P., Mcsween, H. Y., Hibbitts, C. a., Clark, R. N., Pearson, N., & Wang,
704 A. (2013). Nature and degree of aqueous alteration in CM and CI carbonaceous
705 chondrites. *Meteoritics and Planetary Science*, *48*(9), 1618–1637.
706 https://doi.org/10.1111/maps.12171
707 Tatsumi, E., Domingue, D., Yokota, Y., Schroder, S., Hasegawa, S., Kuroda, D., … Sugita,

S. (2020). Global photometric properties of (162173) Ryugu. *Astronomy & Astrophysics*, *639*(37096), A83. https://doi.org/10.1051/0004-6361/201937096

Tonui, E., Zolensky, M., & Lipschutz, M. (2002). Petrography, mineralogy and trace element chemistry of Yamato-86029, Yamato-793321 and Lewis Cliff 85332: Aqueous alteration and heating events. *Antarctic Meteorite Research*, *15*, 38–58. Retrieved from https://ci.nii.ac.jp/naid/110000033028/

Vilas, F. (1994). A Cheaper, Faster, Better Way to Detect Water of Hydration on Solar System Bodies. *Icarus*, *111*(2), 456–467. https://doi.org/10.1006/icar.1994.1156

Vilas, Faith, & Gaffey, M. J. (1989). Phyllosilicate absorption features in main-belt and outer-belt asteroid reflectance spectra. *Science (New York, N.Y.)*, *246*(4931), 790–792. https://doi.org/10.1126/science.246.4931.790

Yamashita, S., Nakamura, T., Jogo, K., Matsuoka, M., & Okumura, S. (2015). Progressive Changes in Mineralogy, Reflectance Spectra and Water Contents of Experimentally Heated Murchison at 400, 600, and 900℃. In *Annual Meeting of the Meteoritical Society* (Vol. 78, p. 5154). Retrieved from https://www.hou.usra.edu/meetings/metsoc2015/pdf/5154.pdf

Table 1. The band centers, depths, reflectances, and slopes of chondrite spectra.

	HS-I		
	Murchison	Murray	Y-793321
3-μm band center of room temperature data (μm)	2.814	2.814	2.931
3-μm band depth of room temperature data	0.513	0.496	0.257
3-μm band center of 120 °C heating data (μm)	2.813	2.805	2.926
3-μm band depth of 120 °C heating data	0.480	0.468	0.173
3-μm band center of 400 °C heating data (μm)	-	-	2.810
3-μm band depth of 400 °C heating data	-	-	0.087
Reflectance at 0.39 μm	0.032	0.028	0.022
Reflectance at 0.55 μm	0.049	0.046	0.030
Reflectance at 0.95 μm	0.052	0.052	0.033
Spectral slope (μm^{-1}) over the 0.39 - 0.95 μm range	0.036	0.043	0.020
0.7-μm band strength	0.066	0.085	-

HS-II			HS-IV		Anhydrous
Jbilet Winselwan	Y 982086	Y 980115	Y-86720	B-7904	Allende
2.717	2.928	2.913	2.957	2.929	2.871
0.242	0.234	0.288	0.276	0.126	0.041
2.719	2.826	2.889	2.915	2.934	2.882
0.241	0.162	0.185	0.213	0.079	0.032
2.717	2.777	2.772	2.886	2.867	2.876
0.227	0.119	0.101	0.097	0.012	0.020
0.026	0.024	0.029	0.048	0.036	0.070
0.040	0.033	0.032	0.062	0.041	0.084
0.044	0.036	0.033	0.060	0.044	0.088
0.032	0.023	0.007	0.022	0.014	0.033
-	-	-	-	-	

Table 2. Summary of mineralogical and spectral changes of Murchison samples experimentally heated at 300,

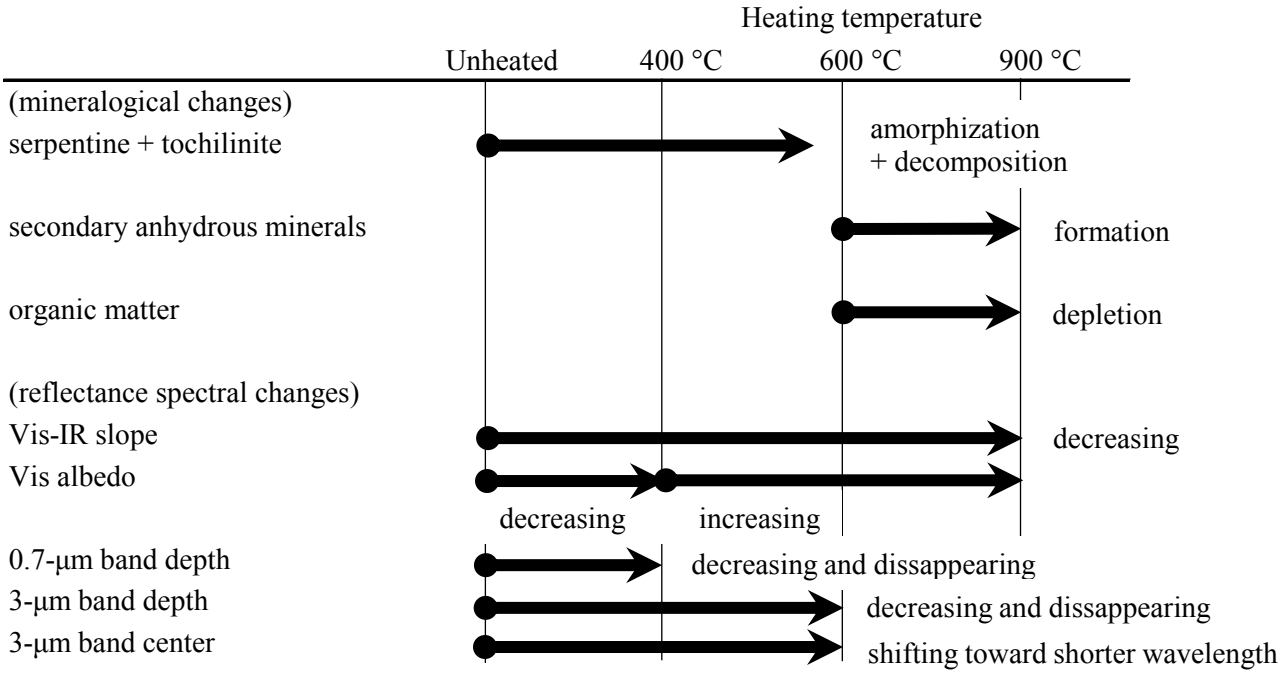

400, 500, 600, and 900 °C reported by Mogi et al. (2017).

Table 3. Summary of mineralogical and spectral changes of carbonace

	Short-duration heating (This study; Matsuoka et al., 2015;2020)
(mineralogical changes)	
serpentine + tochilinite	amorphization
secondary produced materials	formation of FeS-rich amorphous silicate particles
organic matter	carbonazation (possibly occur)
(reflectance spectral changes)	
Vis-IR slope	decrease
Vis albedo	decrease
0.7-μm band depth	decrease
3-μm band depth	decrease
3-μm band center	no change
CF	no change
RB	no change

ous chondrite due to short- and long-duration heating events.

Long-duration heating
(This study; Mogi et al., 2017, 2020 submitted)

---

amorphization,
compositional change (Fe -> Mg)

formation of FeNi-rich metal grains

formation of olivine, pyroxene

depletion

decrease

decrease [from HS-I to II],
increase [to HS-IV]

disappear [at HS-II]

decrease [from HS-I to II],
disappear [at HS-IV]

shift toward shorter
wavelength[from HS-I to II]

shift toward longer wavelength [at HS-IV]

change to olivine feature [at HS-IV]